THE JOURNAL OF PHYSICAL CHEMISTRY B

Article

pubs.acs.org/JPCB

Dependence of Pyranose Ring Puckering on Anomeric Configuration: Methyl Idopyranosides

Benedict M. Sattelle,[†] Bidisha Bose-Basu,[‡,∥] Matthew Tessier,[§] Robert J. Woods,[§,⊥] Anthony S. Serianni,[‡] and Andrew Almond*[,†]

[†]Faculty of Life Sciences, Manchester Interdisciplinary Biocentre, The University of Manchester, 131 Princess Street, Manchester M1 7DN, U.K.

[‡]Department of Chemistry & Biochemistry, University of Notre Dame, 251 Nieuwland Science Hall, Notre Dame, Indiana 46556, United States

[§]Complex Carbohydrate Research Center and Department of Chemistry, University of Georgia, Athens, Georgia 30602, United States.

[⊥]School of Chemistry, National University of Ireland, Galway, University Road, Galway, Ireland

Supporting Information

ABSTRACT: In the aldohexopyranose idose, the unique presence of three axial ring hydroxyl groups causes considerable conformational flexibility, rendering it challenging to study experimentally and an excellent model for rationalizing the relationship between puckering and anomeric configuration. Puckering in methyl α- and β-L-idopyranosides was predicted from kinetically rigorous 10 μs simulations using GLYCAM11 and three explicit water models (TIP3P, TIP4P, and TIP4P-EW). In each case, computed pyranose ring three-bond (vicinal) $^{1}H-^{1}H$ spin couplings ($^{3}J_{H,H}$) trended with NMR measurements. These values, calculated puckering exchange rates and free energies, were independent of the water model. The α- and β-anomers were $^{1}C_4$ chairs for 85 and >99% of their respective trajectories and underwent $^{1}C_4 \rightarrow {}^{4}C_1$ exchange at rates of 20 μs^{-1} and 1 μs^{-1}. Computed α-anomer $^{1}C_4 \leftrightarrow {}^{4}C_1$ puckering rates depended on the exocyclic C6 substituent, comparing hydroxymethyl with carboxyl from previous work. The slower kinetics and restricted pseudorotational profile of the β-anomer were caused by water occupying a cavity bounded by the anomeric 1-*O*-methyl and the C6 hydroxymethyl groups. This finding rationalizes the different methyl α- and β-L-idopyranoside $^{3}J_{H,H}$ values. Identifying a relationship between idopyranose anomeric configuration, microsecond puckering, and water structure facilitates engineering of biologically and commercially important derivatives and underpins deciphering presently elusive structure–function relationships in the glycome.

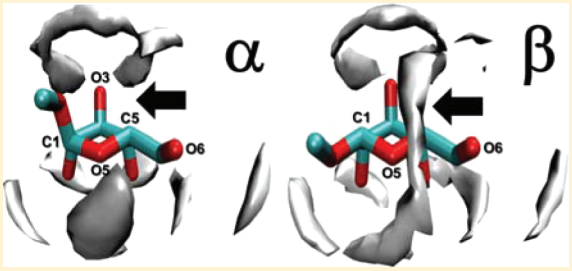

INTRODUCTION

Understanding the conformational dynamics of carbohydrates in aqueous solution is central to rationalizing their plethora of bioactivities. This goal promises to enable structure-based design of new medicines and materials, but its realization remains challenging due to experimental and computational difficulties of probing carbohydrate motions, which occur over a broad range of time scales. Glycosidic linkages librate on nanosecond time scales while pyranose ring conformational exchange (or puckering) and anomerization are microsecond[1] and millisecond time scale phenomena, respectively. The latter process is influenced by the anomeric effect, whose electronic origin remains controversial.[2]

The methyl L-idopyranosides **1** and **2** (Figure 1) are unique among the simple L-aldohexopyranosides because, in the $^{1}C_4$ chair conformation, they exhibit three axial hydroxyl groups at C2, C3, and C4; all other aldohexopyranosides contain a mixture of axial and equatorial hydroxyl substituents at these sites. The idohexopyranosyl ring configuration is thus associated with considerable conformational heterogeneity in water that depends on anomeric configuration.[3] Rationalizing this association could help explain structure–function relationships in the wider glycome (starch and cellulose differ only in their linkage stereochemistry), but it would be difficult to explore in sugars with more stable puckering signatures (e.g., glucose).[4] Idohexopyranoses are important precursors in much needed new approaches to heparan sulfate synthesis.[5] Furthermore, methyl α-L-idopyranosiduronic acid (α-L-IdoA^{-} **3**, Figure 1), a constituent in heparan and dermatan sulfates and the widely used antithrombic drug heparin,[6] was recently predicted[1] to undergo microsecond puckering that depends on substituents and epimerization and is crucial to bioactivity (e.g., anticoagulation).[7]

Received: April 3, 2012
Revised: May 11, 2012
Published: May 11, 2012

dx.doi.org/10.1021/jp303183y | J. Phys. Chem. B 2012, 116, 6380–6386

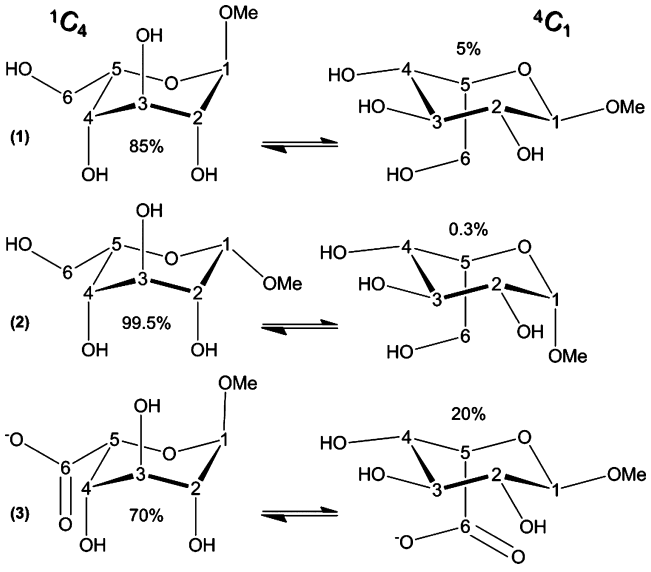

Figure 1. Chair puckers and calculated populations of methyl α- (**1**) and β- (**2**) L-idohexopyranosides studied using 10 μs unbiased explicit solvent molecular dynamics and NMR spectroscopy (D-isomers). Structures and computed populations of methyl α-L-idopyranuronate (**3**), studied previously,[1] are illustrated for comparison.

Prior work has shown that three-bond (vicinal) ^{1}H−^{1}H spin couplings ($^3J_{H,H}$) differ in the α- and β-D-idopyranoses,[3] indicating different conformational equilibria. The distribution of puckers in the α-pyranose may include skew boats in aqueous solution;[3] however, the kinetics of $^1C_4 \leftrightarrow {}^4C_1$ exchange remain unknown. Unfortunately, experimental $^3J_{H,H}$ values provide no kinetic information, and puckering rates derived from previous nonequilibrium picosecond[8] ab initio simulations and nanosecond[9] enhanced sampling molecular dynamics (MD) must be treated with caution since perturbations applied to traverse high (≈8−10 kcal mol^{-1}) free energy barriers associated with chair−chair interconversion distort the kinetics.[10] To better understand puckering dynamics and the effect of C6 substitution in idohexopyranosyl rings and to facilitate exploitation of puckering in structure-based design, we sought to reproduce the experimentally observed dependence of the methyl idopyranoside puckering equilibrium on anomeric configuration using kinetically rigorous microsecond simulations, in which conformational sampling is not artificially enhanced (e.g., by elevated temperature).

Water plays a central role in defining oligosaccharide conformation by influencing the glycosidic linkage structure.[11] The effect of water and different water models on pyranose ring puckering has not been studied previously using microsecond simulations. The present explicit solvent MD (six 10 μs trajectories) converge aqueous puckering in the methyl L-idopyranosides **1** and **2** for the first time. Comparison of these new data with those from a previous 10 μs simulation of **3** shows that idopyranosyl ring $^1C_4 \leftrightarrow {}^4C_1$ exchange kinetics depends on the C6 substituent structure. Predicted $^3J_{H,H}$ values in **1** and **2** trended with NMR measurements made on the D-isomers of **1** and **2** at 750 MHz. These computed properties, calculated chair−chair exchange rates, and relative free energies were unaffected by the type of water potential used in the simulations, comparing three models often used for biomolecular systems:[12] TIP3P,[13] TIP4P,[14] and TIP4P-EW.[15] The experimentally observed puckering behaviors of **1** and **2** were explained by different water structure around each anomer and not by intramolecular steric interactions.

METHODS

Molecular Dynamics. Periodic molecular dynamics simulations of charge-neutral methyl α- and β-L-idopyranosides **1** and **2** were extended to 10 μs using NVIDIA graphics processing units and a development version of ACEMD[16] software (2108). Both monosaccharides were modeled using the GLYCAM11 force field (Supporting Information), each was solvated in an explicit water box of equal side length (28 Å), and three solvent potentials were compared: TIP3P,[13] TIP4P,[14] and TIP4P-EW.[15] Following initial conjugate-gradient energy minimization (1000 steps), each system was heated from 0 to 298 K and equilibrated in the *NPT* ensemble (for 20 ns) prior to 10.25 μs *NVT* production dynamics, the first 250 ns were discarded, and data were recorded at 10 ps intervals. The velocity−Verlet integration algorithm and a hydrogen mass repartitioning scheme allowed a 4 fs time step without affecting the equilibrium distribution.[17] Hydrogen atoms were constrained using the M-SHAKE algorithm,[18] and electrostatic interactions were calculated via the PME method with a grid spacing of 0.9 Å (in the *X*, *Y*, and *Z* dimensions). Electrostatic and van der Waals interactions were truncated at 9 Å, and a scaling factor of 1.0 was employed for carbohydrate 1−4 interactions;[19] the importance of this term has been addressed recently.[20] Gas-phase simulations were performed identically; however, a cubic box of side length 20 Å and a PME grid spacing of 1.0 Å were used.

Calculation of Molecular Properties. All molecular properties were computed using the complete 10 μs trajectories (1 000 000 data points). Puckering was quantified using the Cremer−Pople[21] parameters θ, ϕ, and *Q*, which were derived using the GROMACS[22] analysis tool g_puckering. Relative free energies (ΔG) of binned puckers were calculated using the standard relationship $\Delta G = kT \ln(p_1/p_2)$, where k is the Boltzmann constant, T is temperature (298 K), and p is probability. Puckers were placed in bins of equal area on the Cremer−Pople sphere (unequal spacing in the azimuthal angle θ and equal spacing in the meridian angle ϕ). To achieve this, linear binned values were divided by sin θ to normalize for the area on the sphere (the circumference at azimuthal angle θ is $2\pi r \sin\theta$ on a sphere of radius r). Rotamer populations were computed as described previously,[23] and pyranose ring ^{1}H−^{1}H vicinal spin couplings were calculated using the substituent-adjusted Karplus equations of Haasnoot et al.[24] (see Supporting Information). Radial distribution functions (RDFs) and water densities were derived using the AMBER[25] tool ptraj (keywords "radial" and "grid", respectively). The RDF bin spacing was set to 0.05 Å.

Synthesis of Methyl α- and β-D-Idopyranosides. D-Idose was prepared by cyanohydrin reduction using D-xylose and KCN as substrates.[26] The C2-epimeric products, D-idose and D-gulose, were separated by chromatography on a column (3 cm × 100 cm) containing Dowex 50 × 8 (200−400 mesh) ion-exchange resin in the Ca^{2+} form;[27] idoses eluted first, followed by gulose. D-Idose was converted into the methyl D-idopyranosides by Fischer glycosidation as described previously.[28] After the reaction was complete (~2 h), the resin catalyst was removed by vacuum filtration, and the methanolic solution was concentrated at 30 °C in vacuo to give a syrup. ^{13}C NMR of the syrup in ^2H_2O showed that it contained idofuranosides and idopyranosides, and the 1,6-anhydro

dx.doi.org/10.1021/jp303183y | J. Phys. Chem. B 2012, 116, 6380−6386

derivative (the glycosidation reaction time was kept to a minimum to reduce the amount of the latter). This syrup was dissolved in a minimal amount of distilled water, and the solution was applied to a column (2.5 cm × 100 cm) containing Dowex 1 × 8 (200−400 mesh) ion-exchange resin in the OH^- form.[29] The column was eluted with distilled, decarbonated water, and the effluent was assayed with phenol−sulfuric acid[30] to locate the eluting pyranosides. Careful pooling of fractions gave >95% pure samples of methyl α-D-idopyranoside and methyl β-D-idopyranoside as determined by ^{1}H NMR; the anomers were assigned from their anomeric ^{1}H NMR signal multiplicities by analogy to those reported for α- and β-D-idopyranoses.[3]

NMR Spectroscopy. High-resolution ^{1}H NMR spectra of the methyl α- and β-D-idopyranosides in ^2H_2O were obtained at 750 MHz and 25 °C. Spectra were collected with 2000−3000 Hz sweep widths and 32*K* points, and free induction decays (FIDs) were zero-filled once before processing with resolution enhancement to improve spectral resolution. Since ^{1}H spectra of **1** and **2** were not first-order at 750 MHz, the data were simulated using the MacNUTs program (*MacNUTs Pro*; Acorn NMR Inc., Livermore, CA, USA) to extract accurate chemical shifts and $^3J_{H,H}$ values. Reported ^{1}H chemical shifts (Supporting Information) are accurate to ±0.002 ppm, and reported $^3J_{H,H}$ values (Table 1) are accurate to ±0.2 Hz. The ^{1}H chemical shifts were referenced to the internal residual HOD signal at 4.8 ppm. ^{13}C[^{1}H] NMR spectra of **1** and **2** were obtained at 150 MHz in ^2H_2O and 21 °C. Spectra were collected with 8500 Hz sweep widths and 128k points, and FIDs were zero-filled once before processing with resolution enhancement to improve spectral resolution. ^{13}C chemical shifts (Supporting Information) were referenced externally to the C1 signal of α-D-[1-^{13}C]mannose (95.5 ppm).[31]

RESULTS AND DISCUSSION

Molecular 3D-Properties and Comparison with Experiment. On the basis of our previous metric for conformational convergence (determined by the average value of cos θ, where θ is the Cremer−Pople[21] polar angle),[1] the dynamic 3D-ensemble of ring puckers in **1** and **2** approached the simulation average pucker after approximately 5 μs of explicit solvent MD, irrespective of the water model used (see Supporting Information). Puckering convergence took longer than found previously for net charge-neutral explicit solvent simulations of **3**, methyl 2-*O*-sulfo-IdoA (dianion) and methyl β-D-glucuronate (anion),[1] methyl β-D-glucopyranoside, β-D-galactopyranoside, *N*-acetyl-β-D-galactosaminide, α-D-mannopyranoside and α-L-fucopyranoside,[4] and five methyl and free α-anomer D-hexosamines[23] (the appropriate number of Na^+ counterions were used to neutralize the ensembles). Both **1** and **2** underwent $^1C_4 \leftrightarrow {}^4C_1$ transitions with all three water models, and their average puckers were independent of the water potential (see Supporting Information). In **1**, the average Cremer−Pople[21] pucker parameters θ, φ, and *Q* (see Methods) for $^1C_4$ chairs were 169 ± 6°, 135 ± 70°, and 0.53 ± 0.04; in **2**, these values were 171 ± 6°, 195 ± 80°, and 0.57 ± 0.04, respectively. These results show a larger average value of φ in the β-anomer, indicating a shift from puckers in the ^2S_O-region (φ ≈ 150°) to those in the $^1S_3$-region (φ ≈ 210°). The increased *Q* value in the β-anomer indicates a more chairlike (less flat) pucker relative to the α-anomer. For the $^4C_1$ chairs of **1**, the average θ, φ, and *Q* values were 12 ± 6°, ≈158 ± 100°, and 0.54 ± 0.04; in **2** these values were 14 ± 7°, ≈151 ± 55°, and 0.53 ± 0.04, respectively. The $^4C_1$ chair thus appears to be less sensitive to anomeric configuration than the $^1C_4$ form.

Table 1. Calculated (TIP3P, TIP4P, and TIP4P-EW) and Experimental (EXPT) $^3J_{H,H}$ Values (Hz) for 1 and 2[a]

anomer	$^3J_{H,H}$	TIP3P	TIP4P	TIP4P-EW	EXPT
α	$J_{1,2}$	2.4	2.6	2.6	4.3
α	$J_{2,3}$	2.8	3.0	2.9	6.7
α	$J_{3,4}$	3.1	3.2	3.2	6.1
α	$J_{4,5}$	1.3	1.6	2.8	3.6
β	$J_{1,2}$	1.6	1.7	1.7	1.7
β	$J_{2,3}$	*3.0*	2.9	*2.9*	4.1
β	$J_{3,4}$	3.0	2.9	2.9	4.6
β	$J_{4,5}$	1.1	1.4	*2.8*	2.5

[a]Calculated $^3J_{H,H}$ values were derived from 10 μs trajectories using the substituent-adjusted Karplus equations of Haasnoot et al.[24] Computed and experimental values correspond to L- and D-forms of the sugars, respectively. Calculated values not trending with the experimental data (where the β-anomer $^3J_{H,H}$ value was equal to or greater than the α-anomer $^3J_{H,H}$ value) are italicized.

In the $^1C_4$ pucker of **1** and **2**, all ring vicinal proton−proton pairs are gauche (axial−equatorial or equatorial−equatorial), and therefore relatively small $^3J_{H,H}$ values are expected (≈1−4 Hz). In the $^4C_1$ chair, $^3J_{1,2}$, $^3J_{2,3}$, and $^3J_{3,4}$ in the α-anomer, and $^3J_{2,3}$ and $^3J_{3,4}$ in the β-anomer, correspond to trans (diaxial) coupled protons, and thus large couplings are expected (≈10 Hz). Computed $^3J_{H,H}$ values were in general agreement with these expectations and with prior[3] and new experimental data (Table 1) in that couplings for the α-anomer were larger and thus indicative of a greater proportion of $^4C_1$ form in aqueous solution than found for the β-anomer. Three minor exceptions were noted (italic in Table 1): $J_{2,3}$ (TIP3P and TIP4P-EW) and $J_{4,5}$ (TIP4P-EW), in which the computed $^3J_{H,H}$ values were either identical in both anomers or at most 0.2 Hz greater in the α-anomer (i.e., within the estimated experimental error of ±0.2 Hz). The computed $^3J_{H,H}$ values for the α-anomer were all smaller than the corresponding experimental observations (≈2−4 Hz). In the β-anomer, the maximum difference between calculated and experimental $^3J_{H,H}$ values was ±2 Hz. All computed $^3J_{H,H}$ values were effectively independent of the water model (within 0.2 Hz of each other), except for $^3J_{4,5}$, which differed at most by 1.7 Hz. Although the absolute computed and experimental $^3J_{H,H}$ values for **1** differed by several Hertz, the comparisons in Table 1 provide confidence that the force fields reproduced qualitatively the relative differences between the α- and β-L-idopyranoside equilibrium puckering distributions. The NMR data predicts a more balanced $^1C_4$:$^4C_1$ equilibria than does the MD data (see Supporting Information, two-site models). Improvement of the computed $^3J_{H,H}$ values for the very finely balanced conformational equilibria of **1** and **2** could be achieved via small corrections to force field parameters.

The computed exocyclic hydroxymethyl rotamer populations in **1** and **2** were similar and unaffected by the water models used (Supporting Information). Using the TIP3P water model, the tg:gt:gg states for the α- and β-L-idopyranoside were populated (±1%) at 17:14:69 and 18:8:75, respectively. The experimental populations for the D isomers, in which the gt and gg states are reversed with respect to the L-isomer, were (±5%) 24:0:76 (α-anomer) and 29:4:67 (β-anomer), indicating a slight overestimation of gt in the simulations and faithful

dx.doi.org/10.1021/jp303183y | J. Phys. Chem. B 2012, 116, 6380−6386

representation of the experimentally observed trend for gg ≫ tg > gt.

Puckering Thermodynamics and Kinetics. In the simulations of **1** and **2** using three water models, the $^1C_4$ and $^4C_1$ conformers were the two most populated (lowest energy)

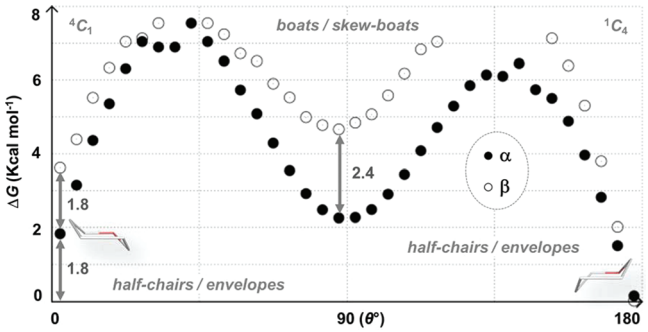

Figure 2. One-dimensional puckering free energy (G) landscapes for **1** and **2** computed from 10 μs explicit solvent (TIP3P) simulations. Free energy differences of $^4C_1$ and equatorial puckers are noted. [This simplified representation facilitates comparison with other sugars. Computed free energies for all sampled canonical puckers are reported in the Supporting Information.]

ring puckers (Figure 2 and Supporting Information). Ratios of $^1C_4$:$^4C_1$ chairs in the α-anomer simulations were 85:5 (TIP3P) and 84:7 (TIP4P) and 84:8 (TIP4P-EW), resulting in computed free energy differences (ΔG) between the two chairs of 1.7 (TIP3P) and 1.4 kcal mol^{-1} (TIP4P and TIP4P-EW). For the β-anomer, the $^1C_4$:$^4C_1$ ratios were 99.5:0.3 (TIP3P), 99.4:0.4 (TIP4P), and 99.8:0.1 (TIP4P-EW) and the computed ΔG values were respectively 3.5, 3.3, ad 3.9 kcal mol^{-1}. In addition to having a higher energy $^4C_1$ pucker, pivotal 3D intermediates in the β-anomer simulation were predicted to have higher free energies when compared to the corresponding α-anomer puckers (Figure 2 and Supporting Information). For example, the lowest energy nonchair puckers in the α- and β-anomer simulations (for all water models) were $B_{1,4}$ and $^5S_1$, respectively, which were ≈2 and ≈4 kcal mol^{-1} higher in free energy cf. $^1C_4$. In the α-anomer, $^5S_1$, $^3S_1$, ^2S_O, and $^1S_3$ puckers were ≤3 kcal mol^{-1} above the $^1C_4$ energy. For the β-anomer, the next lowest energy puckers ($B_{1,4}$, $^{2,5}B$, $^{1,4}B$, and ^2S_O) were predicted to be >5 kcal mol^{-1} above the $^1C_4$ form.

Computed rates of $^1C_4 \leftrightarrow {}^4C_1$ exchange were also independent of the water potential employed (Table 2). Rates for the

Table 2. Calculated Rates of Exchange (μs^{-1}) between Chair Puckers in the Six α- and β-L-Idopyranose 10 μs Simulations

anomer	transition	TIP3P (μs^{-1})	TIP4P (μs^{-1})	TIP4P-EW (μs^{-1})
α	$^1C_4 \rightarrow {}^4C_1$	20.1	19.8	20.4
β	$^1C_4 \rightarrow {}^4C_1$	0.9	0.9	0.7
α	$^4C_1 \rightarrow {}^1C_4$	292.0	200.0	193.0
β	$^4C_1 \rightarrow {}^1C_4$	167.0	149.0	250.0

forward ($^1C_4 \rightarrow {}^4C_1$) transition were 20 and 1 μs^{-1} in the α- and β-anomers, respectively; the backward ($^4C_1 \rightarrow {}^1C_4$) rates were in the ranges of 200−300 μs^{-1} in **1** and 150−250 μs^{-1} in **2**. Our previous simulation of **3** predicted forward and backward rates of 4 and 19 μs^{-1}, respectively.[1] This comparison suggests that the C6 carboxyl substituent of **3** slows the forward and backward puckering exchange rates by approximately 5- and 10-fold, respectively, in idopyranosyl rings.

Puckering Itineraries. Currently, it is not possible to quantify microsecond time scale puckering itineraries using experiments alone. Kinetically rigorous simulations are the best way to improve our understanding of puckering and to complement the burgeoning field of functional glycomics. Previous density functional theory studies of **1** predicted $^1C_4 \leftrightarrow {}^4C_1$ exchange and that the most likely 3D itinerary connects the $^4C_1$ chair and the boat $B_{3,O}$ through the transition-state envelope pucker E_3.[32] A recent metadynamics study found the skew-boat and boat puckers $^1S_3$, $^OS_2$, $^{1,4}B$, and $B_{2,5}$ to be the lowest energy nonchair 3D intermediates in α- and β-D-idopyranose.[9] Our computed puckering free energy landscapes for **1** and **2** were very similar for the TIP3P, TIP4P, and TIP4P-EW water models (see Supporting Information). All 38 canonical puckers (chairs, half-chairs, boats, skew boats, and envelope puckers) were populated in the α-anomer simulations. In the β-anomer simulations, all $^1C_4$-hemisphere puckers were populated; however, specific half-chair and envelope puckers were not explored, including $^4C_1$-hemisphere $^4H_3$, ^4E, and $^4H_5$ ($\theta \approx 30-70°$ and $\phi \approx 210-270°$) and $^1C_4$-hemisphere ^1H_O and ^1E ($\theta \approx 100-140°$ and $\phi \approx 30-90°$) (Figures 3 and 4). Three equatorial puckers, $^{3,O}B$, $^OS_2$, and $B_{2,5}$ ($\theta \approx 70-110°$ and $\phi \approx 0/360$, 330, and 300°), were also precluded in the β-anomer. By inspection of these 3D intermediates, the limited pseudorotational profile and reduced number of interhemisphere transitions in **2** could not be attributed to intramolecular steric hindrance (e.g., between the bulky anomeric 1-*O*-methyl and C6 hydroxymethyl groups). This observation implicates water−pyranose interactions as the cause of the experimentally observed different puckering 3D ensembles of **1** and **2**, with which our calculated $^3J_{H,H}$ values are consistent.

A Role for Water Mediating Idopyranose Microsecond Puckering. Two computed metrics derived from the explicit solvent MD support the hypothesis that the water structure is different around **1** and **2**. First, calculated radial distribution functions (RDFs) for hydrogen-bonding interactions between hydroxyl hydrogen and water oxygen atoms differed in the α- and β-L-idopyranose simulations at the O2 and O4 positions. The relatively decreased peak height in the β-L-idopyranose RDFs at 1.8 Å indicates comparatively fewer solute−solvent hydrogen bonding interactions (cf. α-L-idopyranose) in the first hydration shell at both positions (Figure 5). The inequalities observed in the second solvation shell trended similarly and also indicate a different water structure at O2 and O4. Integration of the RDFs in the first shell (1.0 to 2.5 Å) showed the presence of 0.55 and 0.48 water molecules in the α- and β-anomers, respectively. In the second shell (3.0 to 5.0 Å), the respective water occupancy was computed to be and 1.14 and 1.05. No differences were observed in RDFs computed for interactions between water oxygen atoms and hydroxyl hydrogen atoms at the pyranose O3 and O6 positions.

Second, the computed water density in close proximity to the solute, over the lifetime of the 10 μs trajectories, was different in the simulations of **1** and **2**. Inequalities were observed in the computed water densities using the TIP3P solvent model, with the most significant difference being the greater propensity of water to cluster in the cavity bounded by the anomeric 1-*O*-methyl substituent and the C6 hydroxymethyl group in the β-anomer, compared to the α-anomer (Figure 6). The explicit solvent simulations therefore suggest that water molecules

dx.doi.org/10.1021/jp303183y | J. Phys. Chem. B 2012, 116, 6380−6386

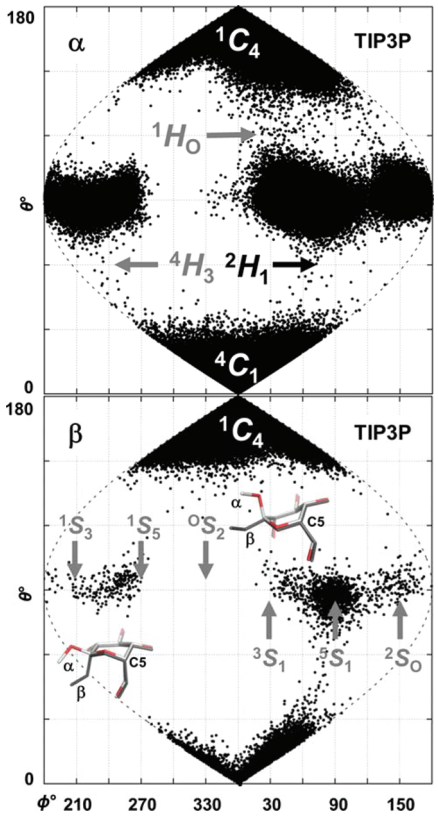

Figure 3. Sinusoidal projection of computed puckering in **1** (top) and **2** (bottom). [Data are from 10 μs simulations using GLYCAM11 and the TIP3P solvent model. All sampled puckers are shown. Predicted 3D intermediates linking chair and equatorial puckers in the α-anomer (^1H_O and $^4H_3$) which were precluded in the β-anomer simulation, are indicated in gray (top). Models of these puckers (α- and β-anomers) are shown at their respective positions in puckering space on the β-anomer plot (bottom), in which equatorial skew-boat (S) puckers are labeled above/below their respective positions (gray). By inspection of these overlaid 3D structures, it is apparent that no intermolecular steric hindrance results from anomerization. Analogous plots for TIP4P and TIP4P-EW water models are reported in the Supporting Information.]

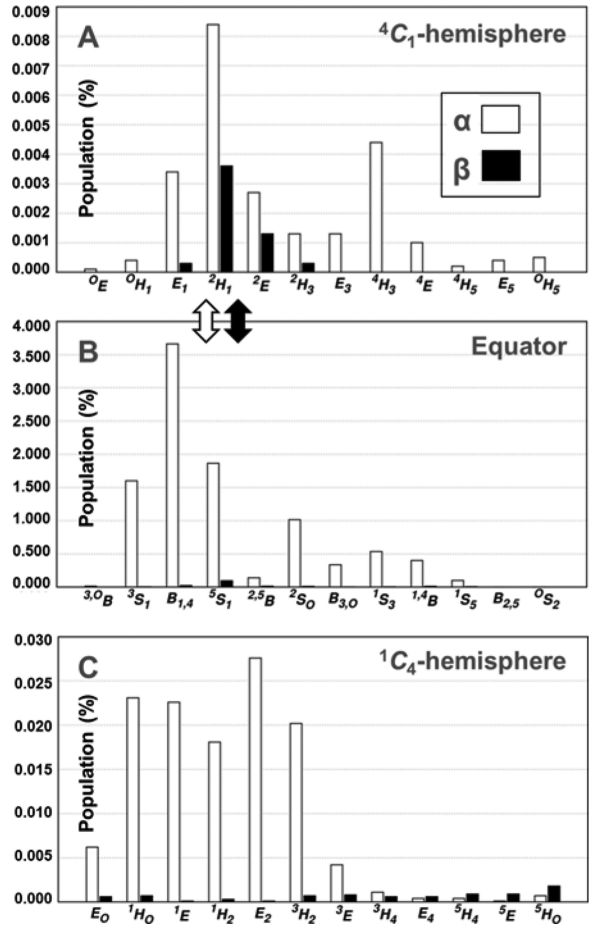

Figure 4. Histograms showing the occupancy of pyranose puckers for (**1**) and (**2**) in the $^4C_1$-hemisphere (A), equatorial region (B), and $^1C_4$-hemisphere (C) during 10 μs simulations (TIP3P water model). [The most likely transitions (based on pucker populations) between the equator and the $^4C_1$-hemisphere are denoted by arrows. Multiple conformational itineraries between the equator and the $^1C_4$-hemisphere were predicted for **1**; e.g., $B_{1,4} \leftrightarrow {}^1E$.]

present within this cavity in the β-L-idopyranoside slow the microsecond kinetics of pyranose puckering.

This hypothesis was further supported by analysis of 10 μs periodic gas-phase MD data for **1** and **2**. The principal difference from the explicit solvent MD was a 3-fold increase in the computed forward $^1C_4 \rightarrow {}^4C_1$ transition rate in the β-anomer, computed to be 1 μs^{-1} in the aqueous MD and 3 μs^{-1} in the gas phase (Supporting Information). Calculated α-anomer $^1C_4 \rightarrow {}^4C_1$ puckering rates were identical in the water and gas-phase MD. This finding is consistent with the proposal that water structure causes the slower puckering kinetics of the β-anomer, compared to the α-anomer. Together, these predictions rationalize the smaller measured and calculated $^3J_{H,H}$ values in the β-anomer (cf. the α-anomer). Mechanistically, the explicit solvent MD findings suggest that water molecules limit the capacity of the β-anomer to adopt the 3D intermediates ^1H_O and $^4H_3$ highlighted in Figure 3.

CONCLUSIONS

Pyranose ring puckering is crucial to carbohydrate−protein interactions and concomitant bioactivity, exemplified by the heparin−antithrombin III interaction,[7] which initiates anti-coagulation. Previous work has shown that pyranose substituents and chiral configurations (epimers) impact microsecond-puckering kinetics.[1,4,23] To further understand the effects of stereochemical changes on puckering, here we used flexible idopyranosides as a model to explore the dependence of pyranose microsecond-exchange on anomeric configuration, which is also a key regulator of bioactivity (e.g., glycan−lectin[33] binding).

The aqueous simulations described herein explain the different experimentally observed puckering ensembles in **1** and **2** and reveal intermediate puckers that are less favorable in the β-anomer compared to the α-anomer, in water. Comparison with a previous[1] explicit solvent 10 μs simulation of methyl α-L-idopyranuronate **3** intimated that conversion of the C6 carboxyl group to a hydroxymethyl group in an α-L-idopyranosyl ring significantly increases the forward ($^1C_4 \rightarrow {}^4C_1$) and backward ($^4C_1 \rightarrow {}^1C_4$) puckering exchange rates by 5- and 10-fold, respectively. On the basis of previous work concerning the effect of 1-*O*-methylation on aqueous monosaccharide microsecond puckering,[23] we anticipate that the free reducing idopyranoses will exhibit different puckering 3D ensembles from those seen in the simulations of **1** and **2**. The effect of C6

dx.doi.org/10.1021/jp303183y | J. Phys. Chem. B 2012, 116, 6380−6386

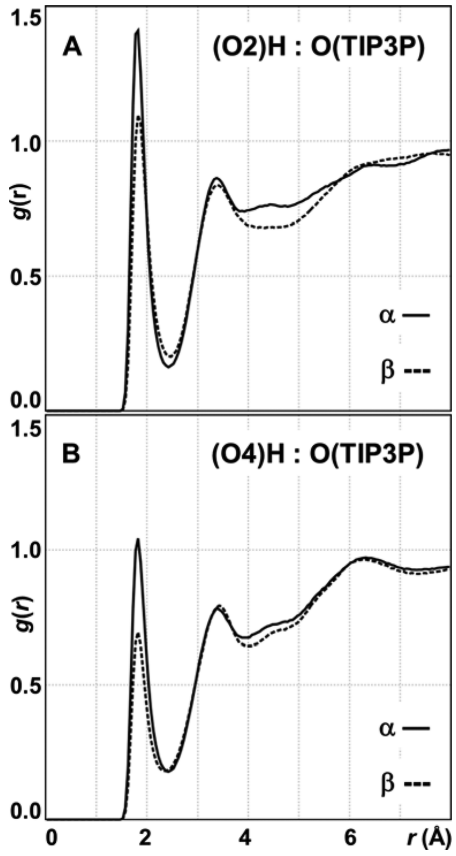

Figure 5. Radial distribution functions for the through-space interaction of TIP3P water oxygen atoms and hydroxyl hydrogen atoms at the α (**1**) and β (**2**)-L-idohexopyranosyl ring positions O2 (A) and O4 (B).

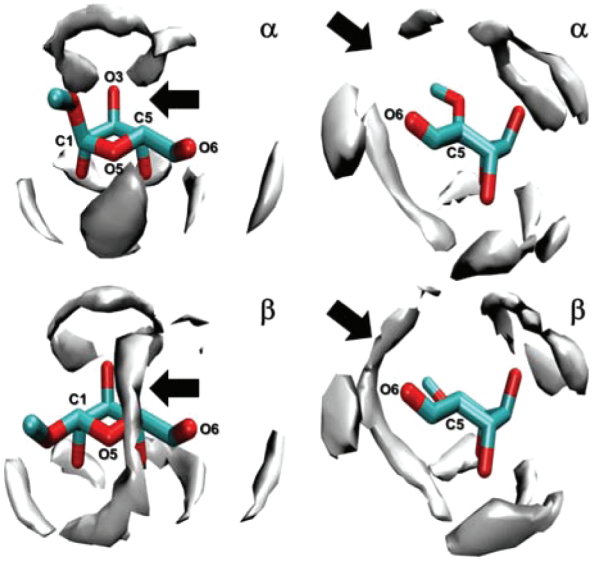

Figure 6. Isosurface representations of computed water densities surrounding **1** and **2** during 10 μs explicit solvent (TIP3P) simulations. [Two views of each anomer, in the $^1C_4$ pucker, are shown. The cavity bounded by the anomeric 1-*O*-methyl substituent and the C6-hydroxymethyl group is indicated by an arrow.]

substitution in the free reducing idopyranoses also remains to be studied.

The present work reaffirms the role of water as a major contributor to carbohydrate 3D structure,[11] suggesting that water determines pucker populations and chair−chair exchange kinetics, and also provides evidence that three- and four-site water models perform similarly with respect to computed microsecond-puckering 3D-structural, kinetic, and thermodynamic properties. It will likewise be informative to test the performance of simpler (e.g., implicit) and more complex (e.g., five-site) water models when such simulations become practical on the time scales required to converge pyranose puckering (≈2−5 μs).[1,4,23] The observation that water structure plays a role in pyranose microsecond-puckering kinetics can be exploited to help engineer exchange rates and bioactivity. For example, substituents that stabilize potential biologically important puckers in **1**, **2**, **3**, and structurally related molecules can be studied in silico on microsecond time scales and in water, prior to synthesis and biological testing. In this regard, biologically relevant, kinetically rigorous and experimentally validated microsecond simulations, such as those reported here, are an important step toward deciphering glycomic structure−function relationships and rational design of new carbohydrate-based medicines and materials.

■ ASSOCIATED CONTENT

Supporting Information

Tables listing rank conformer populations and free energies, deviations of computed Cremer−Pople parameters, hydroxymethyl rotamer state populations, pyranose ring vicinal couplings, two-site models, chemical shifts, classification of nonchair puckers, coupling calculations, dihedral averages, and GLYCAM11 parameters and figures showing 3D definitions of hydroxymethyl conformations, convergence of pucker, time series of the Cremer−Pople parameter, projections of spherical phase space, relative occupancy of puckers, and synthesis reaction schemes. This information is available free of charge via the Internet at http://pubs.acs.org.

■ AUTHOR INFORMATION

Corresponding Author

*E-mail: Andrew.Almond@manchester.ac.uk. Tel.: +44 (0)161 306 4199. Fax: +44 (0)161 306 5201.

Present Address

[‖]Department of Chemistry and Physics, Fayetteville State University, Fayetteville, NC 28301, USA.

Notes

The authors declare no competing financial interest.

■ ACKNOWLEDGMENTS

The authors gratefully acknowledge M. J. Harvey and G. De Fabritiis (acellera.com) for enabling use of a development version of ACEMD software. A.A. and B.M.S. wish to acknowledge that this work was supported by funding from the Biotechnology and Biological Sciences Research Council (Grant BB/G006768/1). R.J.W. thanks the National Institutes of Health (Grants P41RR005351, P41GM103390, and GM094919 (EUREKA)) as well as the Science Foundation of Ireland (Grant 08/IN.1/B2070) and the European Research Development Fund for support.

REFERENCES

(1) Sattelle, B. M.; Hansen, S. U.; Gardiner, J.; Almond, A. Free Energy Landscapes of Iduronic Acid and Related Monosaccharides. *J. Am. Chem. Soc.* **2010**, *132*, 13132−13134.

(2) (a) Wang, C.; Ying, F.; Wu, W.; Mo, Y. Sensing or No Sensing: Can the Anomeric Effect Be Probed by a Sensing Molecule? *J. Am. Chem. Soc.* **2011**, *133*, 13731−13736. (b) Mo, Y. Computational Evidence That Hyperconjugative Interactions Are Not Responsible for the Anomeric Effect. *Nat. Chem.* **2010**, *2* (8), 666−671.

(3) Snyder, J. R.; Serianni, A. S. D-Idose—A One-Dimensional and Two-Dimensional NMR Investigation of Solution Composition and Conformation. *J. Org. Chem.* **1986**, *51*, 2694−2702.

(4) Sattelle, B. M.; Almond, A. Assigning Kinetic 3D-Signatures to Glycocodes. *Phys. Chem. Chem. Phys.* **2012**, *14* (16), 5843−5848.

(5) Reichardt, N. C.; Czechura, P.; Guedes, N.; Kopitzki, S.; Vazquez, N.; Martin-Lomas, M. a New Linker for Solid-Phase Synthesis of Heparan Sulfate Precursors by Sequential Assembly of Monosaccharide Building Blocks. *Chem. Commun. (Cambridge, U.K.)* **2011**, *47* (8), 2390−2392.

(6) Liu, H.; Zhang, Z.; Linhardt, R. J. Lessons Learned from the Contamination of Heparin. *Nat. Prod. Rep.* **2009**, *26* (3), 313−321.

(7) Hricovini, M.; Guerrini, M.; Bisio, A.; Torri, G.; Petitou, M.; Casu, B. Conformation of Heparin Pentasaccharide Bound to Antithrombin III. *Biochem. J.* **2001**, *359* (Pt 2), 265−272.

(8) Schnupf, U.; Willett, J. L.; Momany, F. DFTMD Studies of Glucose and Epimers: Anomeric Ratios, Rotamer Populations, and Hydration Energies. *Carbohydr. Res.* **2010**, *345* (4), 503−511.

(9) Autieri, E.; Sega, M.; Pederiva, F.; Guella, G., Puckering Free Energy of Pyranoses: A NMR and Metadynamics-Umbrella Sampling Investigation. *J. Chem. Phys.* **2010**, *133* (9).

(10) Schlick, T. Molecular Dynamics-Based Approaches for Enhanced Sampling of Long-Time, Large-Scale Conformational Changes in Biomolecules. *F1000 Biol. Rep.* **2009**, *1*, No. 51.

(11) (a) Kirschner, K. N.; Woods, R. J. Solvent Interactions Determine Carbohydrate Conformation. *Proc. Natl. Acad. Sci. U. S. A.* **2001**, *98* (19), 10541−10545. (b) Corzana, F.; Motawia, M. S.; Du Penhoat, C. H.; Perez, S.; Tschampel, S. M.; Woods, R. J.; Engelsen, S. B. A Hydration Study of (1→4) and (1→6) Linked Alpha-Glucans by Comparative 10 ns Molecular Dynamics Simulations and 500-MHz NMR. *J. Comput. Chem.* **2004**, *25* (4), 573−586. (c) Corzana, F.; Motawia, M. S.; Herve du Penhoat, C.; van den Berg, F.; Blennow, A.; Perez, S.; Engelsen, S. B. Hydration of the Amylopectin Branch Point. Evidence of Restricted Conformational Diversity of the α-(1→6) Linkage. *J. Am. Chem. Soc.* **2004**, *126*, 13144−13155.

(12) Jorgensen, W. L.; Tirado-Rives, J. Potential Energy Functions for Atomic-Level Simulations of Water and Organic and Biomolecular Systems. *Proc. Natl. Acad. Sci. U. S. A.* **2005**, *102* (19), 6665−6670.

(13) Jorgensen, W. L.; Chandrasekhar, J.; Madura, J. D.; Impey, R. W.; Klein, M. L. Comparison of Simple Potential Functions for Simulating Liquid Water. *J. Chem. Phys.* **1983**, *79* (2), 926−935.

(14) Jorgensen, W. L.; Madura, J. D. Temperature and Size Dependence for Monte-Carlo Simulations of Tip4p Water. *Mol. Phys.* **1985**, *56* (6), 1381−1392.

(15) Horn, H. W.; Swope, W. C.; Pitera, J. W.; Madura, J. D.; Dick, T. J.; Hura, G. L.; Head-Gordon, T. Development of an Improved Four-Site Water Model for Biomolecular Simulations: TIP4P-Ew. *J. Chem. Phys.* **2004**, *120* (20), 9665−9678.

(16) Harvey, M. J.; Giupponi, G.; De Fabritiis, G. ACEMD: Accelerating Biomolecular Dynamics in the Microsecond Time Scale. *J. Chem. Theory Comput.* **2009**, *5*, 1632−1639.

(17) Buch, I.; Harvey, M. J.; Giorgino, T.; Anderson, D. P.; De Fabritiis, G. High-Throughput All-Atom Molecular Dynamics Simulations Using Distributed Computing. *J. Chem. Inf. Model* **2010**, *50*, 397−403.

(18) Krautler, V.; Van Gunsteren, W. F.; Hunenberger, P. H. A Fast SHAKE: Algorithm To Solve Distance Constraint Equations for Small Molecules in Molecular Dynamics Simulations. *J. Comput. Chem.* **2001**, *22* (5), 501−508.

(19) Kirschner, K. N.; Yongye, A. B.; Tschampel, S. M.; Gonzalez-Outeirino, J.; Daniels, C. R.; Foley, B. L.; Woods, R. J. GLYCAM06: A Generalizable Biomolecular Force Field. Carbohydrates. *J. Comput. Chem.* **2008**, *29* (4), 622−655.

(20) Spiwok, V.; Kralova, B.; Tvaroska, I. Modelling of β-D-Glucopyranose Ring Distortion in Different Force Fields: A Metadynamics Study. *Carbohydr. Res.* **2010**, *345* (4), 530−537.

(21) Cremer, D.; Pople, J. A. General Definition of Ring Puckering Coordinates. *J. Am. Chem. Soc.* **1975**, *97*, 1354−1358.

(22) Hess, B.; Kutzner, C.; van der Spoel, D.; Lindahl, E. GROMACS 4: Algorithms for Highly Efficient, Load-Balanced, and Scalable Molecular Simulation. *J. Chem. Theory Comput.* **2008**, *4*, 435−447.

(23) Sattelle, B. M.; Almond, A. Is *N*-Acetyl-D-glucosamine a Rigid $^4C_1$-Chair? *Glycobiology* **2011**, *21* (12), 1651−1662.

(24) Haasnoot, C. A. G.; Deleeuw, F. A. A. M.; Altona, C. The Relationship between Proton-Proton NMR Coupling-Constants and Substituent Electronegativities—1. An Empirical Generalization of the Karplus Equation. *Tetrahedron* **1980**, *36* (19), 2783−2792.

(25) Case, D. A.; Cheatham, T. E., 3rd; Darden, T.; Gohlke, H.; Luo, R.; Merz, K. M., Jr.; Onufriev, A.; Simmerling, C.; Wang, B.; Woods, R. J. The Amber Biomolecular Simulation Programs. *J. Comput. Chem.* **2005**, *26* (16), 1668−1688.

(26) (a) Serianni, A. S.; Nunez, H. A.; Barker, R. Carbon-13-Enriched Carbohydrates−Preparation of Aldononitriles and Their Reduction with a Palladium Catalyst. *Carbohydr. Res.* **1979**, *72* (Jul), 71−78. (b) Serianni, A. S.; Vuorinen, T.; Bondo, P. B. Stable Isotopically-Enriched D-Glucose - Strategies to Introduce Carbon, Hydrogen and Oxygen Isotopes at Various Sites. *J. Carbohydr. Chem.* **1990**, *9* (5), 513−541.

(27) Angyal, S. J.; Bethell, G. S.; Beveridge, R. J. Complexes of Carbohydrates with Metal Cation. 10. Separation of Sugars and of Polyols on Cation-Exchange Resins in the Calcium Form. *Carbohydr. Res.* **1979**, *73* (Aug), 9−18.

(28) Podlasek, C. A.; Wu, J.; Stripe, W. A.; Bondo, P. B.; Serianni, A. S. [^{13}C]-Enriched Methyl Aldopyranosides: Structural Interpretations of ^{13}C-^{1}H Spin-Coupling Constants and ^{1}H Chemical Shifts. *J. Am. Chem. Soc.* **1995**, *117*, 8635−8644.

(29) Austin, P. W.; Baddiley, J.; Hardy, F. E.; Buchanan, J. G. Separation of Isomeric Glycosides on Basic Ion-Exchange Resins. *J. Chem. Soc.* **1963**, No. Nov, 5350−5353.

(30) Hodge, J. E.; Hofreiter, B. T. Determination of Reducing Sugar and Carbohydrate. *Methods Carbohydr. Chem.* **1962**, *1*, 380−394.

(31) King-Morris, M. J.; Serianni, A. S. ^{13}C NMR-Studies of [1-^{13}C]Aldoses: Empirical Rules Correlating Pyranose Ring Configuration and Conformation with ^{13}C Chemical Shifts and ^{13}C/^{13}C Spin Couplings. *J. Am. Chem. Soc.* **1987**, *109*, 3501−3508.

(32) Kurihara, Y.; Ueda, K. an Investigation of the Pyranose Ring Interconversion Path of Alpha-L-Idose Calculated Using Density Functional Theory. *Carbohydr. Res.* **2006**, *341* (15), 2565−2574.

(33) Gabius, H. J. Glycans: Bioactive Signals Decoded by Lectins. *Biochem. Soc. Trans.* **2008**, *36* (Pt6), 1491−6.